Magnetic flux distribution in a three-dimensional inductive network of Josephson junctions

A. Tuohimaa,* J. Paasi, and T. Tarhasaari
Laboratory of Electromagnetics, Tampere University of Technology, FIN-33101 Tampere, Finland

T. Di Matteo and R. De Luca
INFM–Dipartimento di Fisica, Universitá degli Studi di Salerno, I-84081 Baronissi (Salerno), Italy
(Received 28 October 1998; revised manuscript received 20 October 1999)

The magnetic response of three-dimensional Josephson junction networks to constant or slowly varying external magnetic fields is studied. General equations are written for complex networks made of *n* elementary cubic cells, each cell containing 12 resistively shunted ideal Josephson junctions. The magnetic-flux distribution in the network is calculated numerically as a function of the external magnetic field for different values of superconducting quantum interference device parameter, network size, and external magnetic-field direction. The magnetic-flux distribution in the network is graphically shown, first for increasing and then for decreasing values of the external magnetic flux.

I. INTRODUCTION

Josephson-junction networks (JJN's) have been extensively studied in the last few years. The electromagnetic properties of these systems have become of interest after the discovery of high-temperature superconductivity. The interest in JJN's derives both from their potential technological application as superconducting devices[1] and from their use as model systems in the study of electromagnetic properties of high-T_C granular superconductors.[2]

It has been proposed that three-dimensional (3D) JJN's can be used as vectorial magnetic-field sensors,[3] so that they might open new perspectives in the realm of superconducting devices. Moreover, 3D JJN's may be used as a model to study the electromagnetic behavior of weakly coupled granular superconductors. The networks can provide a picture of the magnetic-flux distribution in the intergranular regions of these materials, which is more realistic than that provided by one or two dimensional JJN's. Indeed, the 3D JJN may open a new viewpoint into the three-dimensional magnetization of the superconducting bulk materials and help understand the bulk effects. Several research groups have already studied the 3D JJN's in the limit of negligible magnetic energy.[4–7] However, regions may exist on the *H-T* plane where this limit does not apply as, for example, in the case of granular superconductors with μm-size intergranular defects in the low-field and low-temperature limit. Here the magnetic energy of the induced currents should be taken into account.

Equations for the inductive 3D JJN were originally derived by Nakajima and Sawada.[8] We have recently studied the static magnetic response of an elementary cubic network[9] and derived analytic expressions for the lower threshold field of linearly aligned cubes[10] by using circulating loop currents with inductances. However, in the 3D JJN's the loop currents become ineffective, since they are no more unique.

In this paper, a simple JJN model of the elementary cube[9] is expanded to more complex inductive 3D JJN's, consisting of *n* elementary cubes. The magnetic-flux distribution and the magnetic-moment density of the system are studied. The model is based on the inductive effects of the branch currents, which in turn can be uniquely solved from magnetic fluxes. We present a few chosen examples with the aim of finding the main characteristics of the magnetic behavior of inductive 3D JJN's. The paper is organized as follows: The model is presented in Sec. II and the main results are discussed in Sec. III. Conclusions are drawn in the last section with a special emphasis on the main characteristics of 3D networks of inductively coupled Josephson-junction networks.

II. MODEL

The JJN model under study consists of elementary cubic subnetworks, which we shall call ''cubes.'' One of the cubes is sketched in the bottom right corner of the JJN shown in Fig. 1(a). We denote the number of cubes in the *x*, *y*, and *z* direction with n_x, n_y, and n_z, respectively, so that $n = n_x n_y n_z$ is the total number of cubes. In the following, the structure of the network is identified by using the notation $n_x \times n_y \times n_z$. Each cube has 12 Josephson junctions, one on each edge, as shown in Fig. 1(b). Between two adjacent cubes there are four shared junctions and one face with a magnetic flux in common. Let now the vector **r** define a

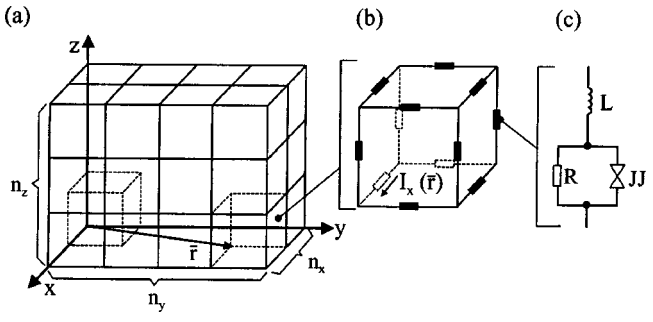

FIG. 1. Circuital inductive three-dimensional Josephson-junction network model. (a) Network made of $n = n_x n_y n_z$ cubes. (b) Elementary cubic Josephson-junction network with current variables. (c) Box containing inductance *L* and ideal Josephson junction JJ, shunted with resistance *R*.

point in $\mathbb{R}^3$ and the vectors $\mathbf{v}_1$, $\mathbf{v}_2$, and $\mathbf{v}_3$ form a right-handed basis in $\mathbb{R}^3$. A cell is defined as an object consisting of a point $\mathbf{r}$ and of the three unitary vectors $\{\mathbf{v}_1,\mathbf{v}_2,\mathbf{v}_3\}$ so that any point of the cell is given by $\mathbf{r}+\alpha_1\mathbf{v}_1+\alpha_2\mathbf{v}_2+\alpha_3\mathbf{v}_3$, where $0\leqslant\alpha_1,\alpha_2,\alpha_3\leqslant a$, with a being the lattice constant. The cell is denoted by $C_{v_1v_2v_3}(\mathbf{r})\equiv\{\mathbf{r},\mathbf{v}_1,\mathbf{v}_2,\mathbf{v}_3\}$ with the orientation given by the positional order of $\{\mathbf{v}_1,\mathbf{v}_2,\mathbf{v}_3\}$. Correspondingly, a face can be represented by the collection of the vectors $f_{v_1v_2}(\mathbf{r})\equiv\{\mathbf{r},\mathbf{v}_1,\mathbf{v}_2\}$. Choosing a Cartesian coordinate system, one can identify the faces by the vector $\mathbf{r}$ and by the indices $(\mu\nu)=(xy)$, (zx), or (yz). Thus, as in Ref. 9, we write the magnetic flux across the face $\{\mathbf{r},\boldsymbol{\mu},\boldsymbol{\nu}\}$ as $\phi_{\mu\nu}(\mathbf{r})$. Likewise, $I_\mu(\mathbf{r})$ stands for the branch current through a junction $\{\mathbf{r},\boldsymbol{\mu}\}$.

We assume that all junctions are identical and overdamped. The resistively shunted junction (RSJ) model is used to describe their behavior: ideal Josephson junctions are characterized by a phase difference and the maximum Josephson current I_J, and they are shunted by a resistance R [Fig. 1(c)]. The gauge-invariant phase difference of the junction lying along the $\hat{\xi}$ ($\hat{x}$, $\hat{y}$, or $\hat{z}$) direction in the cell at the position $\mathbf{r}$ is named by $\varphi_\xi(\mathbf{r})$. Now, by letting the nonlinear Josephson operator O_J,

$$O_J(\cdot)=\frac{\phi_0}{2\pi R}\frac{d}{dt}(\cdot)+I_J\sin(\cdot), \tag{1}$$

act upon the phase difference $\varphi_\xi(\mathbf{r})$ and by setting the result equal to the current flowing through the junction, we can write the equations of motion

$$O_J[\varphi_\xi(\mathbf{r})]=I_\xi(\mathbf{r}). \tag{2}$$

The relations between the normalized flux variables $\Psi=\phi/\phi_0$ and the superconducting phase differences are obtained from the flux quantization condition for each closed face in the network:

$$2\pi\Psi_{(\mu\nu)}(\mathbf{r})=2\pi p_{(\mu\nu)}(\mathbf{r})+\varphi_\nu(\mathbf{r}+a\hat{\mu})-\varphi_\nu(\mathbf{r})-\varphi_\mu(\mathbf{r}+a\hat{\nu})+\varphi_\mu(\mathbf{r}), \tag{3}$$

where the $p_{\mu\nu}(\mathbf{r})$'s are integer coefficients.

The flux quantization equations can be written for all the faces by introducing a translation operator $\hat{T}_\eta$, where the index η gives the direction along which the translation is performed. The operator acts directly upon the position vector $\mathbf{r}$. For example, when applied to the phase differences, it acts in the following way:

$$\hat{T}_\eta\varphi_\xi(\mathbf{r})=\varphi_\xi(\mathbf{r}+a\hat{\eta}). \tag{4}$$

Similarly $\hat{T}_\eta$ acts upon the fluxes $\Psi_{(\mu\nu)}(\mathbf{r})$, the currents $I_{(\mu)}(\mathbf{r})$, and the flux numbers $p_{(\mu\nu)}(\mathbf{r})$, as in Eq. (4).

If the applied magnetic field strength $\mathbf{H}$ is assumed to be homogeneously distributed over the network, the equation $\mathbf{B}=\mu_0(\mathbf{M}+\mathbf{H})$ defines linkage between the magnetic-flux density $\mathbf{B}$ and the magnetization $\mathbf{M}$. The equation relates the branch currents and the fluxes as follows: The fluxes $\phi_{\mu\nu}(\mathbf{r})$ can be calculated from the line integral $\oint\mathbf{A}(\mathbf{r})\cdot d\mathbf{l}+\mu_0\mathbf{H}\cdot\mathbf{S}_{(\mu\nu)}(\mathbf{r})$, where the line integral is taken around the face $\{\mathbf{r},\boldsymbol{\mu},\boldsymbol{\nu}\}$, $\mathbf{A}(\mathbf{r})$ is the magnetic vector potential due to branch currents, and $\mathbf{S}_{(\mu\nu)}(\mathbf{r})$ is the area vector pertaining to the cube face located at the position $\mathbf{r}$ and orthogonal to the $(\mu\nu)$ plane. By dividing the line integral in pieces, according to the branches belonging to the loop, we may write $\oint_f\mathbf{A}(\mathbf{r})\cdot d\mathbf{l}=\Sigma_{b:es}\int_b\mathbf{A}(\mathbf{r})\cdot d\mathbf{l}$, where *b:es* are the branches belonging to the boundary of f. For $b=\{\mathbf{r},\hat{\mu}\}$ the term $\int_b\mathbf{A}(\mathbf{r})\cdot d\mathbf{l}$ can in turn be obtained from the integral

$$\int_0^a\mathbf{A}_\mu(\mathbf{r})\cdot d\mathbf{l}=\frac{\mu_0}{4\pi}\sum_{r'}\int_0^a\frac{I_\mu(\mathbf{r}')d\mathbf{l}_\mu(\mathbf{r}')}{d_{l(r),l(r')}}\cdot d\mathbf{l}_\mu(\mathbf{r}),$$

where $d_{l(r),l(r')}$ is the distance between the components $\mathbf{l}_\mu(\mathbf{r})$ and $\mathbf{l}_\mu(\mathbf{r}')$. By defining a partial mutual inductance, as in Ref. 11,

$$M^p_{(\mu)}(\mathbf{r},\mathbf{r}')=\frac{\mu_0}{4\pi}\int_0^a\int_0^a\frac{d\mathbf{l}_\mu(\mathbf{r})\cdot d\mathbf{l}_\mu(\mathbf{r}')}{d_{l(r),l(r')}}, \tag{5}$$

the integral can be written as $\int_0^a\mathbf{A}_\mu(\mathbf{r})=\Sigma_{r'}M^p_{(\mu)}(\mathbf{r},\mathbf{r}')I_\mu(\mathbf{r}')$. In this case, the magnetic flux can be calculated by completing the circulation and by adding the external magnetic field contribution, as follows:

$$\phi_{(\mu\nu)}(\mathbf{r})=\sum_{\mathbf{r}'}\{M^p_{(\mu)}(\mathbf{r},\mathbf{r}')I_{(\mu)}(\mathbf{r}')-M^p_{(\mu)}(\mathbf{r}+a\hat{\nu},\mathbf{r}')\times I_{(\mu)}(\mathbf{r}')+M^p_{(\nu)}(\mathbf{r},\mathbf{r}')I_{(\nu)}(\mathbf{r}')-M^p_{(\nu)}(\mathbf{r}+a\hat{\mu},\mathbf{r}')\times I_{(\nu)}(\mathbf{r}')\}+\mu_0\mathbf{H}\cdot\mathbf{S}_{(\mu\nu)}(\mathbf{r}). \tag{6}$$

The $M^p_{(\mu)}(\mathbf{r},\mathbf{r}')$ coefficients are solved analytically for one-dimensional wires (cf. Appendix A for details). Equations (6) can be expressed in matrix from as $\tilde{\Phi}=\mathbf{PMI_b}$, where $\tilde{\Phi}=\phi_{(\mu\nu)}(\mathbf{r})-\mu_0\mathbf{H}\cdot\mathbf{S}_{(\mu\nu)}(\mathbf{r})$ contains both the magnetic flux and the external field contribution, $\mathbf{P}$ is the matrix denoting the summation, $\mathbf{M}$ contains the corresponding $M^p_\mu(\mathbf{r},\mathbf{r}')$ terms, and $\mathbf{I_b}$ is a column vector whose components are the branch currents.

Equations (1)–(6) form a set of nonlinear ordinary differential equations that applies generally to inductive 3D JJN's. The boundary of a specific network is obtained by requiring that the currents outside the network are zero.

We use the fourth-order Runge-Kutta method (RK4) to solve the above set of equations. In order to obtain the magnetic flux and the current distribution in the network, for each step of the RK4 we start by calculating the fluxes from the phase differences, Eq. (3), and then solve the branch currents from the fluxes by using Eq. (6). Because the matrix $[\mathbf{PM}]$ is rank-deficient, the inverse problem will be discussed in more detail in Appendix B. Finally, we substitute the branch currents in Eq. (2); in this way, Eq. (2) becomes a set of coupled nonlinear differential equations for the phase differences φ_ξ's.

Since $\mathbf{H}$ is considered to be homogeneously distributed over the network knowing the magnetic-flux distribution in the loops, we can calculate the discretized magnetization, i.e., the magnetization for each loop to obtain

$$M_\xi(\mathbf{r})=\frac{1}{\mu_0 S_{(\mu\nu)}(\mathbf{r})}\phi_{(\mu\nu)}(\mathbf{r})-H_\xi, \tag{7}$$

where $\xi\perp(\mu,\nu)$. Finally, the magnetization is averaged as

$$m_\xi = \frac{1}{n_f} \sum_{\mathbf{r}} \frac{1}{\mu_0 S_{(\mu\nu)}(\mathbf{r})} \phi_{(\mu\nu)}(\mathbf{r}) - H_\xi, \tag{8}$$

where n_f is the number of the loops.

III. RESULTS

We study here the magnetic response of zero-field-cooled (ZFC) networks of size $8\times8\times8$ by means of the procedure set forth in the preceding section. The external magnetic field is increased with small increments in order to simulate realistic magnetic-field sweeps. For computational purposes, a normalized external flux $\psi_e = 2\pi\mu_0|\mathbf{H}||\mathbf{S}|/\phi_0$ is defined. After each increase of $\Delta\psi_e = 0.1\pi$, the system is allowed to relax close to its stationary solution. If not otherwise stated, the relaxation time Δt after each increase of $\Delta\psi_e$ is $\Delta t = 100 l/R$, where l is a partial self inductance of a branch, and l/R is the natural time unit of the JJN (typically of size 10^{-10}–10^{-12} s). Finally, the calculated magnetic flux and current distributions are recorded before the external field is again increased by $\Delta\psi_e$.

In the following, we shall examine flux penetration mainly in the loops parallel to the *xy* plane. These loops form layers characterized by the ratio $k = r_z/a$, which defines the orientation and the position of the layer in space. The directions of the external magnetic field are chosen in such a way that the flux distribution in the *xz* and *yz* layers can be deduced from that in the *xy* layers. Thus we show the flux distribution for the (*xy*) faces and cut off the other faces for simplicity. For the clarity the spacing of the *xy* layers in the figures is larger than the spacing in the network. The values representing the magnetic fluxes in phases $\psi = 2\pi\phi/\phi_0$ are given on the gray-color scale sketched at the bottom of the figures.

Like one- and two-dimensional JJN's (cf. Refs. 12–14), the 3D JJN can be in either a reversible or an irreversible state, and the irreversible state can again be either a network vortex or a network critical state, depending on the superconducting quantum interference device (SQUID) parameter of the system. These states resemble their analogous partners in type-II superconductors. The network critical and vortex states will be discussed in the following, in the context of the 3D JJN.

At low values of the external magnetic field, no magnetic flux penetrates irreversibly into the ZFC system, and the magnetic flux decays exponentially from the edge to the center of network, and therefore we call such a state a reversible state. As the magnetic flux begins to penetrate, the parameter $\beta = 2\pi l I_J/\phi_0$ defines the kind of state that is formed in the network. Due to analogy we refer to the parameter β as a SQUID parameter, although it is defined for a branch not for a loop. With high β values a network critical state is formed in the system, whereas at low β values a network vortex state occurs.

A. Network critical state

Let us now study the magnetic-flux distribution in the $8\times8\times8$ network for the value $\beta = 2\pi$ and the field direction $\hat{H} = (0,0,1)$. In Fig. 2, magnetic-flux distributions are shown for the increasing external field values $\psi_e = 3\pi$ (a), $\psi_e = 6\pi$ (b), $\psi_e = 10\pi$ (c); finally, the remanent magnetic-flux distribution is presented in (d). When the first threshold field is exceeded, the magnetic flux begins to penetrate the top and bottom layers, as shown in Fig. 2(a). After a phase-slip process, the magnetic flux has penetrated into the system in the form of Josephson network vortices (JNV), which are seen as the dark-gray spots in the layers $k = 0$ and $k = 8$ in Fig. 2(a). In this case [$\hat{H} = (0,0,1)$, $\psi_e = 3\pi$, and $\beta = 2\pi$] eight JNV's penetrate the system, Fig. 2(a), two from each perimetrical side, and they are localized almost entirely in one loop with the neighboring loops only slightly affected by the penetrating flux. The parameter value $\beta = 2\pi$ is high enough to allow for the network critical state, and in this case the magnetic flux is indeed trapped in the loops next to the edge of the network. Three dimensionality here affects the shielding properties of the system. Indeed, considerably less magnetic flux penetrates the center layers $k = 3$–5 than the top and bottom layers in Fig. 2(a). As the external field is further increased, more flux penetrates into the network with arrow-like flux fronts as shown in Figs. 2(b) and (c). Taking one layer, we note that resembling flux fronts occurs also in 2D JJN's (Ref. 15) and in rectangular superconductors.[16,17]

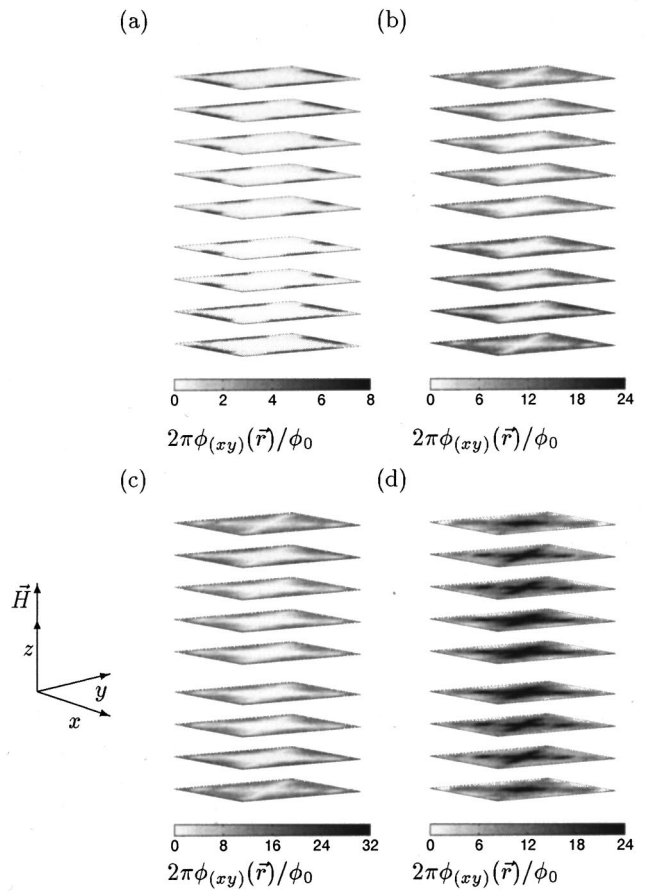

FIG. 2. Magnetic-flux distributions in $8\times8\times8$ network for $\beta = 2\pi$, $\hat{H} = (0,0,1)$. (a) $\psi_e = 3\pi$, (b) $\psi_e = 6\pi$, (c) $\psi_e = 10\pi$, and (d) remanent magnetic-flux distribution, $\psi_e = 0$.

Due to magnetic coupling, the screening effects are the strongest in the center layers, resulting in the bending of the JNV's. Even at $\psi_e = 10\pi$, which is enough to produce a full penetration in the $k = 0$ and $k = 8$ layers in Fig. 2(c), a flux

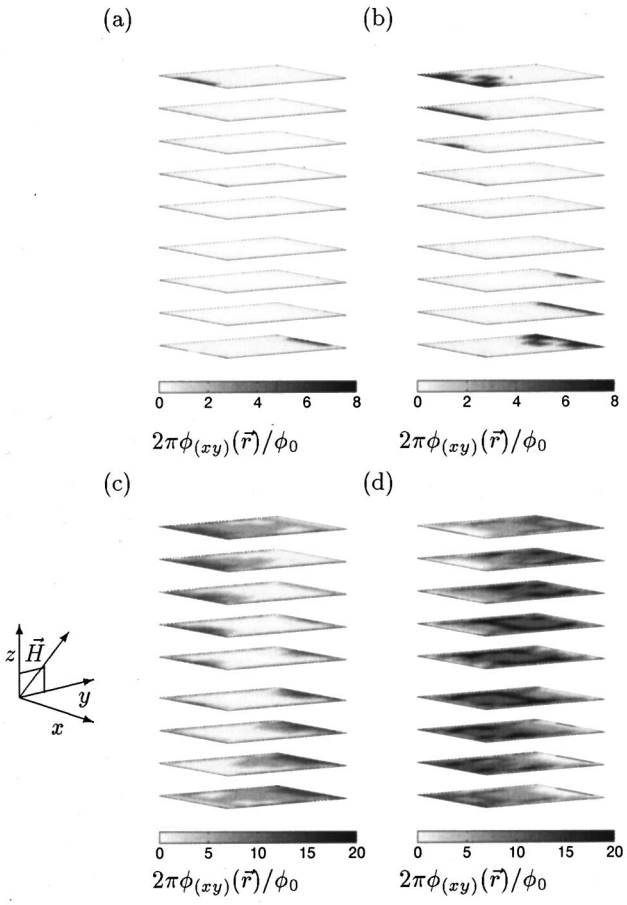

FIG. 3. Magnetic-flux distributions in $8\times8\times8$ network for $\beta=2\pi$, $\hat{H}=(0,1/\sqrt{2},1/\sqrt{2})$. (a) $\psi_e=2\pi$, (b) $\psi_e=3\pi$, (c) $\psi_e=6\pi$, and (d) remanent magnetic-flux distribution, $\psi_e=0$.

free region exists in the center of the layers $k=1-7$. Such bending has been found also in type-II superconductors of finite thickness by E. H. Brandt, by means of a theoretical critical state approach.[18]

After the maximum value $\psi_e=15\pi$ is obtained, the ψ_e is decreased, and the magnetic flux begins to flow outward from the middle of the side faces. A further decrease in ψ_e results in further magnetic flux flowing out from the side faces, in accordance with the critical state model.[19] Finally, at $\psi_e=0$, the remanent flux is pinned into the network, as shown in Fig. 2(d), with most of it pinned in the center layers. The remanent magnetic-flux distribution in a single layer resembles that obtained in a 2D JJN with a complete mutual inductive matrix.[15]

Let us now consider the field direction $\hat{H}=(0,1/\sqrt{2},1/\sqrt{2})$. We take a snapshot of an $8\times8\times8$ network with $\beta=2\pi$ for the field values $\psi_e=2\pi$, 3π, 6π, and finally, for the remanent magnetic-flux distribution, $\psi_e=0$, in Figs. 3(a)–(d), respectively. At $\psi_e=2\pi$ (a), some junctions in the network have undergone a phase-slip process. The magnetic-field direction defines the places where the magnetic flux enters the JJN. In the case of $\hat{H}=(0,1/\sqrt{2},1/\sqrt{2})$, these areas lie on the sides $(n_x,j,0)$ and $(0,j,n_z)$, with $j=0\cdots7$, of the xy layers $k=0$ and $k=n_z$, respectively. The sides form a kind of outmost rim for the external flux. On these edges the shielding currents in the xy and yz layers with

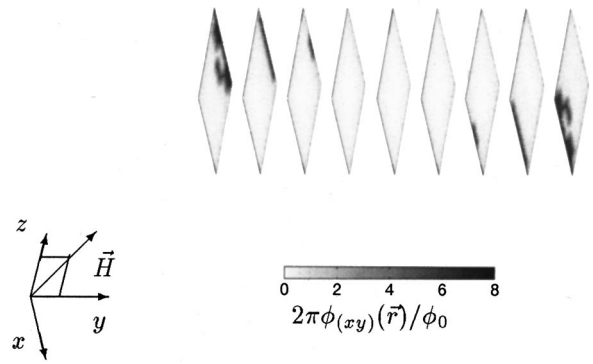

FIG. 4. Magnetic-flux distributions in xz layers, in $8\times8\times8$ network for $\beta=2\pi$, $\hat{H}=(0,1/\sqrt{2},1/\sqrt{2})$, and $\psi_e=3\pi$.

a common branch flow in the same direction, and the maximum Josephson current is first exceeded in junctions located on these sides, whereas on the opposite edges the screening currents are opposite and cancel each other. For the case in Fig. 2(a), two JNV's penetrated the network symmetrically from each side, whereas here the penetration occurs only through two edges.

As for the direction $\hat{H}=(0,0,1)$ [Figs. 2(b) and (c)], also in $\hat{H}=(0,1/\sqrt{2},1/\sqrt{2})$ an increase in ψ_e causes the magnetic flux to penetrate the network with an arrowlike distribution [Figs. 3(b) and (c)]. The entering vortices have their magnetic moment parallel to the external field, which can be seen by comparing the Figs. 4 and 3(b). In Fig. 4, the magnetic flux distribution is shown for xz layers for the case above with $\psi_e=3\pi$. Evidently, the location of the dark-gray areas shifts as one goes from the bottom xy layer denoted by $k=0$ to the next xy layer with $k=1$ [Fig. 3(b)]. Similar flux distribution is also present in xz layers. The shielding of the inner cells of the network, lying along lines parallel to the applied magnetic field, is obvious in this case, for only little magnetic flux is present in the centers of the middle layers [Figs. 3(b) and (c)]. Let us, finally, look at the remanent magnetic-flux distribution, Fig. 3(d). After the field is swept back to zero from its maximum $\psi_e=15\pi$, the magnetic flux leaves the sides where the penetration started. A considerable amount of flux, however, is trapped in the center of the network.

B. Network vortex state

The number of loops over which a single JNV spreads depends on the SQUID parameter. This can be deduced by comparing Figs. 2 and 5. In Fig. 5, magnetic-flux distribution is shown for the $8\times8\times8$ network with $\beta=1$ for the external flux $\psi_e=0.7\,\pi$ (a), and the remanent magnetic-flux distribution $\psi_e=0$ (b), and with $\beta=0.1$ for external flux $\psi_e=0.4\pi$ (c), and the remanent magnetic-flux distribution $\psi_e=0$, (b), respectively. The direction of the external field was chosen to be $\hat{H}=(0,0,1)$ to allow comparison with Fig. 2.

Because at values $\beta=0.1$ and 1 one mesh can trap only a small amount of magnetic flux, the JNV overlaps several loops with the overlap larger for $\beta=0.1$ than for $\beta=1$. Consequently, in both cases the flux is distributed over a large area. In fact, in the case of $\beta=0.1$, the magnetic flux is more equally distributed over one layer of the JJN. In addition, at

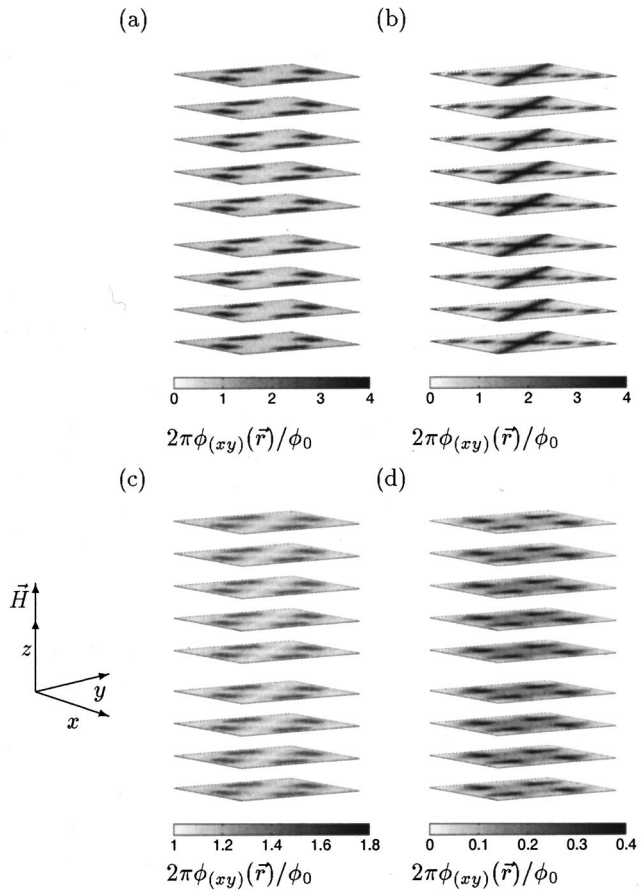

FIG. 5. Magnetic-flux distributions in $8\times8\times8$ network for $\hat{H}=(0,0,1)$ with $\beta=1$ for (a) $\psi_e=0.7\pi$, (b) remanent magnetic-flux distribution, $\psi_e=0$, and with $\beta=0.1$ for (c) $\psi_e=0.4\pi$, (d) remanent magnetic-flux distribution, $\psi_e=0$.

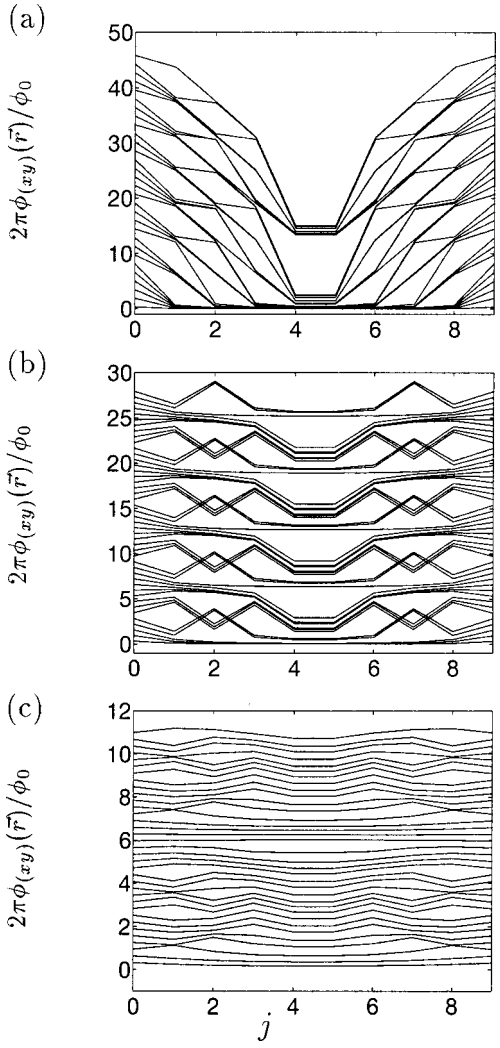

FIG. 6. Magnetic-flux profiles of $8\times8\times8$ network as a function of j for values $k=5$ and $i=5$, and for $\hat{H}=(0,0,1)$. Here ψ_e increases from zero and used β values are (a) $\beta=2\pi$, (b) $\beta=1$, and (c) $\beta=0.1$.

field values just above $\psi_{\rm th}$, the lower threshold field of the network, the penetrated JNV's are not located in the corners but at the center of the sides. This vortex distribution resembles that reported in two-dimensional networks by Chen, Moreno, and Hernando.[20] The first threshold field is found to be in between $0.3\pi<\psi_{\rm th}<0.4\pi$ for $\beta=0.1$, and $0.6\pi<\psi_{\rm th}<0.7\pi$ for $\beta=1$. Finally, for $\hat{H}=(0,0,1)$, and $\beta=0.1$ and 1, the magnetic flux is almost equally distributed in adjacent layers. Furthermore, no clear signs of the network critical state is found in the remanent flux distribution for $\beta=1$ and $\beta=0.1$, [Figs. 5(b) and (d)]; instead, the spacing of the trapped JNV's clearly depends on the β value. Seemingly a network vortex state prevails.

For a detailed look at the transition between the network critical and vortex state, we present the magnetic-flux distribution profiles of $8\times8\times8$ network at $k=5$, $i=5$, and $j=[0\cdots7]$ in Fig. 6 for β values of 2π, 1, and 0.1 in (a), (b), and (c), respectively. The corresponding increasing ψ_e values are added to both ends; hence the index j runs from $j=0,1,2,...,9$. We notice that for $\beta=2\pi$ [Fig. 6(a)], the magnetic-flux distribution is a piecewise continuous curve with a nonzero average gradient. This is analogous to what has been found in 1D and 2D JJN's.[14,12] Because the flux profiles display behavior reminiscent of the Bean critical state model, we can argue that, besides local deviations, a network critical state has been established in the JJN. Furthermore, at full flux penetration the profiles periodically repeat the same shapes of local deviations as a function of ψ_e, the period being $\Delta\psi_e=4\pi$.

In the case $\beta=0.1$ [Fig. 6(b)], the system shows an average gradient close to zero and ψ oscillates as a function of j so that the network vortex state prevails. In the network vortex state, the oscillating flux component is the only component present. Here the vortex trapping is due only to the current flowing at the edges, i.e., the trapping is caused by the surface barrier. However, with $\beta=1$, the network might have a finite average gradient, as also supported by magnetization studies (Sec. III C). We note, that in $8\times8\times8$ networks the transition from the network vortex state to network critical state is smooth, such that both a network vortex state and a network critical state behavior may be present depending on external flux value at $\beta\approx1$. At a growing β, the vortex state is less and less likely to occur and finally disappears altogether.

C. Magnetization of the network

Finally, we analyze the magnetic moment density **m** of the $8\times8\times8$ network defined by Eq. (8). In Fig. 7, the mag-

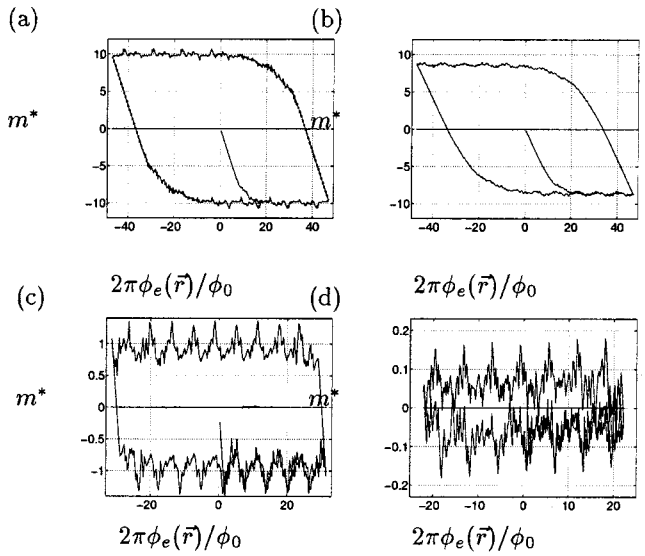

FIG. 7. Scaled magnetic moment density of $8\times8\times8$ network as a function of $\psi_e=2\pi\phi_e(\mathbf{r})/\phi_0$ for three cases: $\beta=2\pi$ (a) and (b), $\beta=1$ (c), and $\beta=0.1$ (d). Field direction $\hat{H}=(0,0,1)$ for (a) (b) (c) and $\hat{H}=(0,1/\sqrt{2},1/\sqrt{2})$ for (b).

netic moment density of the system is plotted as a function of the external field for values $\beta=2\pi$ (a) and (b), $\beta=1$ (c), and $\beta=0.1$ (d), and for the field directions $\hat{H}=(0,0,1)$ (a), (c) (d) and $\hat{H}=(0,1/\sqrt{2},1/\sqrt{2})$ (b). Note that **m** is scaled by a factor $2\pi\mu_0 S/\phi_0$ such that $m^*=\|2\pi\mu_0 S\mathbf{m}/\phi_0\|$. With the highest SQUID parameter value, $\beta=2\pi$, the system evinces strong magnetization (a) and (b), and, except for a slight ripple, the magnetization curve resembles that in Bean's critical state model.[19] The maximum magnetization of the sample is weaker for the field direction $\hat{H}=(0,1/\sqrt{2},1/\sqrt{2})$ than for $\hat{H}=(0,0,1)$. The periodicity of the magnetization as a function of the external magnetic flux also changes with a changing field direction, as seen by comparing the curves (a) where $\Delta\psi_e=4\pi$ and (b) where $\Delta\psi_e=2\sqrt{2}\pi$. Generally, the periodicity differs from that of a 1D or 2D JJN with the difference caused by the mutual inductive coupling of branches, as shown in Fig. 7(a), where the period is $\Delta\psi_e=4\pi$. At $\beta=1$, both the oscillation of m^* as a function of the external field and its maximum absolute value are enhanced, the periodicity now being $\Delta\psi_e=2\pi$, as shown in Fig. 7(a), and thus similar to that of a 2D JJN.[21] At about these β values, the 3D JJN undergoes a smooth transition between the network critical and the vortex state. For example, neglecting the ripple a nonzero magnetization component prevails, indicating that a network with $\beta=1$ still has magnetic flux pinned inside the network. Thus, at $\beta=1$, the network has neither a clear network vortex state nor a network critical state but is in a regime of transition. When $\beta=0.1$, the magnetic-moment density of the network is small, indicating weak screening effects. Maximum magnetization occurs at $\Delta\psi_e=2\pi$ periods, and oscillation, caused by surface barrier pinning, is then clearly present.

IV. DISCUSSION

For SQUID parameters sufficiently high we found that the network screens its inner part from external magnetic flux. This behavior results in a network critical state. At increasing fields, clear flux fronts are present and the magnetic-flux penetration starts in the middle of the side faces. Comparing the magnetic-flux distribution and the magnetic hysteresis curves of the 3D JJN with the experiments on Bi-2223 polycrystalline samples,[22–25] we found that the high-β simulations of the 3D JJN give results which qualitatively agree with the experimental results. The above suggests that a 3D JJN with high β is a valid model to describe qualitatively the low-field magnetic properties of a granular sample.

A quantitative comparison between calculations and experiments is difficult because real polycrystalline samples consist of myriads of grains with varying intergranular properties; therefore the results in this paper are tentative, and further studies are required in for more specific results on the magnetic response of a 3D JJN and on the applicability of these models for the study of the low magnetic-field behavior of granular superconductors. More detailed studies on a 3D JJN as a model for the intergranular magnetic properties of high-temperature superconductor bulks would have to include additional features such as structural disorder as well as coupling inhomogeneities.

V. CONCLUSIONS

We expanded existing inductive JJN models to 3D JJN's made of cubic subnetworks. To show the main characteristics of the magnetic behavior of small networks, we presented the magnetic-flux distribution in the $8\times8\times8$ networks for cycling external magnetic fields with fixed field directions.

We found that the networks screen their inner parts from external magnetic flux, provided that the SQUID parameter is sufficiently high, whereas weak shielding is detected for low SQUID parameter values. For external magnetic fields higher than the lower threshold field of the network, the magnetic flux enters into the system in the form of Josephson network vortices whose magnetic moments have favorably the same direction as the external magnetic field. These vortices tend to penetrate deeper into the network as the external magnetic field is increased. The behavior is to some extent analogous to the penetration of magnetic flux into type-II superconductors.[26]

Finally, even though further studies are required to establish a quantitative agreement between the magnetic response of 3D JJN's and granular superconductors, we believe that these model systems are natural candidates for the detailed study low-field magnetic-flux penetration in polycrystalline superconducting samples.

We thank Professor L. Kettunen at Tampere University of Technology, and Professor S. Pace at University of Salerno for helpful discussions. A.T. also wishes to express his gratitude to Finnish Academy of Science and Letters for support.

APPENDIX A: INDUCTANCE CALCULATIONS

Adopting a 3D (Josephson-junction) network as a model to study the electromagnetic properties of a real granular system, we should bear in mind that the currents depicted in the circuit in Fig. 1 describe only the currents which effectively flow into the junctions. In this way the current distri-

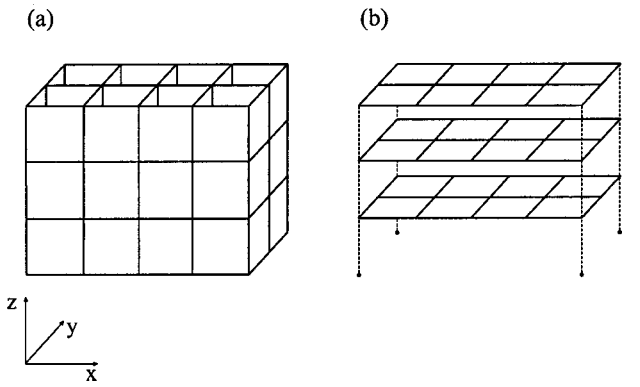

FIG. 8. (a) Choice of tree of facets made for cubic network and (b) its co-tree.

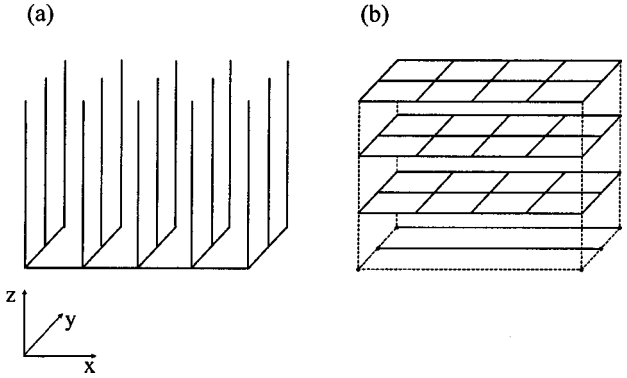

FIG. 9. (a) Choice of tree of edges made for cubic network and (b) its co-tree.

bution in Fig. 1 does not reproduce the actual current distribution of the physical system. However, a complete treatment of the physical system is rather involved since the shielding currents circulating at the grain surfaces are not easy to calculate and only a portion of the superficial current density flows through the junctions. Therefore we shall consider only the simple case of the network shown in Fig. 1.

Since the loop current method proved ineffective with the 3D network, we developed, in Sec. II and Appendix B, a method using branch currents. Mutual inductive coupling was then taken into account by introducing a partial mutual inductance, Eq. (5). Here we consider the calculation of the inductances. In the beginning, we note that all the branches in the network in Fig. 1 are either perpendicular or parallel to each other. Because in the Neuman formula [27] the perpendicular components vanish, in the following, it is enough to deal with two parallel current blocks at a time. Let us consider two one-dimensional wires 1 and 2 of length a placed in the μ direction and being a distance of $d_{(\nu,\eta)}$ apart from each other on (ν,η) plane with centers d_μ apart in μ direction. We obtain

$$m_{\mathrm{par}}=\frac{\mu_0}{4\pi}\int_0^a\int_{a_\mu}^{a+d_\mu}\frac{dl_1dl_2}{\sqrt{d_{\nu,\eta}^2+(l_1-l_2)^2}}, \tag{A1}$$

which is solved analytically.

However, if the branches $(\mu)(\mathbf{r})$ and $(\mu)(\mathbf{r}')$ refer to the same location $(\mathbf{r}=\mathbf{r}')$, the integrand in the integral, which gives the coefficient $M^P_{(\mu)}(\mathbf{r},\mathbf{r}')$, is singular. To solve this problem we may first consider the self-inductances of a current loop. Each face of the cube can be thought to contain a square current loop made of thin cylindrical wire of diameter $2r$ and the side length a. The self-inductance of the whole loop is then given by[15,27]

$$I_{\mathrm{loop}}=\frac{\mu_0 a}{4\pi}\left(2+8\left(\ln\frac{2a}{r(1+\sqrt{2})}+\sqrt{2}-2\right)\right). \tag{A2}$$

Each loop can be divided into four branches, each with a partial self-inductance l and a negative mutual contribution from the opposite branch m_{par} such that $L_{\mathrm{loop}}/4=l-m_{\mathrm{par}}$. Therefore the partial self-inductance for the branches can be obtained from

$$l=L_{\mathrm{loop}}/4+\frac{\mu_0}{4\pi}[2a-2\sqrt{2a^2}+2a\sinh^{-1}(1)], \tag{A3}$$

where the second part on the right is to eliminate the mutual inductive effect of the opposite branch in the loop. For $a=10\,\mu$m and $2r=0.1\,\mu$m, l is 9.097×10^{-12} H. Using the method above, we calculated the partial mutual inductance in among all the branches and built up a matrix **M** which was then used for 3D JJN, as described in Sec. II.

APPENDIX B: UNIQUE SOLUTION OF THE FLUX CURRENT LINKAGE

As stated previously, Eq. (6), which links the magnetic flux and branch currents, is underdetermined. Indeed, the magnetic flux $\tilde{\Phi}$ has linearly dependent components. In this case the linear dependence arises from the Maxwell equation $\nabla\cdot\mathbf{B}=0$, which implies that over each closed surface A enclosing a volume V we must have

$$\int_A(\mathbf{B}\cdot\mathbf{n})dA=0, \tag{B1}$$

where **n** is the normal component of the differential surface dA. Equation (B1) means that the magnetic flux coming into the volume V must be equal to the outflowing flux. Consequently, each cube has one face whose magnetic flux can be described in terms of the fluxes across the other faces. Let us now turn to the currents. Unlike with the loop current method, Eqs. (1)–(6) do not imply the Kirchoff's current rule to hold for the branch currents. Instead, it has to be explicitly required. According to the rule one of the branch currents can be expressed in terms of the other currents at each node.

To make the solutions unique we may proceed as follows using simple network theory:[28–30] At first, we can remove the linearly dependent fluxes from the flux vector $\tilde{\Phi}$. The fluxes through the faces can be calculated by introducing a tree and a co-tree in the cubic network. A facet tree is a maximal set of facets (=cubic faces) without any cycles, where the cycle is a set of facets without a boundary.[31] Such a tree can be made, e.g., in the way shown in Fig. 8.

Now each cofacet (i.e., co-tree facet) closes a surface with some volume within. Therefore a flux through any facet on the co-tree can be expressed in terms of the facets on the tree belonging to the path of the co-facet in question. Hence lin-

early dependent fluxes can be eliminated by omitting the fluxes belonging to the co-tree, by removing the corresponding components from $\tilde{\Phi}$ and the corresponding rows from **P**.

Since the branch currents have to obey Kirchhoff's current rule, we introduce a tree and co-tree on the cubic edges, Fig. 9. All the branch currents, satisfying the current rule, can be computed by solving the branch currents on the edges belonging to the co-tree. In matrix form we write

$$\mathbf{I_b} = \begin{bmatrix} \mathbf{Q} \\ \mathbf{I} \end{bmatrix} \mathbf{I_{ct}}, \tag{B2}$$

where a row of **Q** gives a branch current belonging to the tree as a function of branch currents belonging to the co-tree, **I** is identity matrix, and $\mathbf{I_{ct}}$ is the currents on the co-tree. The number of the edges on the co-tree is the same as the amount of the facets on the facet tree.

Finally, the inverse problem can be written as

$$\tilde{\Phi} = \left[\mathbf{PM} \begin{bmatrix} \mathbf{Q} \\ \mathbf{I} \end{bmatrix} \right] \mathbf{I_{ct}}, \tag{B3}$$

where the matrix in outer brackets is invertible. Having solved $\mathbf{I_{ct}}$, we can finally obtain the branch currents from Eq. (B2).

*Electronic address: tuohimaa@cc.tut.fi

[1] *Handbook of Applied Superconductivity*, edited by B. Seeber (IOP Publishing, Bristol, 1998).

[2] J. R. Clem, Physica C **153-155**, 50 (1988).

[3] T. Di Matteo, J. Paasi, A. Tuohimaa, and R. De Luca, IEEE Trans. Appl. Supercond. **9**, 3515 (1999).

[4] C. J. Lobb, D. W. Abrahams, and M. Tinkham, Phys. Rev. B **27**, 150 (1983).

[5] C. Ebner and D. Stroud, Phys. Rev. B **31**, 165 (1985); W. Yu and D. Stroud, *ibid.* **51**, 3725 (1995).

[6] E. A. Jagla and C. A. Balseiro, Phys. Rev. B **52**, 4494 (1995); **55**, 3192 (1997).

[7] M. A. Zelikman, Supercond. Sci. Technol. **10**, 795 (1997); **12**, 1 (1999); **12**, 187 (1999).

[8] J. Nakajima and Y. Sawada, J. Appl. Phys. **52**, 5732 (1981).

[9] R. De Luca, T. Di Matteo, A. Tuohimaa, and J. Paasi, Phys. Rev. B **57**, 1173 (1998).

[10] T. Di Matteo, J. Paasi, A. Tuohimaa, and R. De Luca, Phys. Lett. A **247**, 360 (1998).

[11] J. R. Phillips, H. S. Van der Zant, H. S. J. White, and T. P. Orlando, Phys. Rev. B **47**, 5219 (1993).

[12] F. Parodi and R. Vaccarone, Physica C **173**, 56 (1991).

[13] D.-X. Chen, A. Sanchez, and A. Hernando, Physica C **250**, 107 (1995).

[14] D.-X. Chen, J. J. Moreno, and A. Hernando, Phys. Rev. B **53**, 6579 (1996).

[15] D. Reinel, W. Dieterich, T. Wolf, and A. Majhofer, Physica C **245**, 193 (1995).

[16] T. Schuster, H. Kuhn, E. Brandt, and S. Klaumuenzer, Phys. Rev. B **56**, 3413 (1997).

[17] M. R. Koblischka and R. J. Wijngraaden, Supercond. Sci. Technol. **8**, 199 (1995).

[18] E. H. Brandt, Phys. Rev. B **54**, 4246 (1996).

[19] C. P. Bean, Rev. Mod. Phys. **36**, 31 (1964).

[20] D.-X. Chen, J. Moreno, and A. Hernando, Phys. Rev. B **56**, 2364 (1997).

[21] D. Dominquez and J. V. José, Phys. Rev. B **53**, 11 692 (1996).

[22] A. Oota, K. Kawano, K. Fujikawa, and H. Fujimoto, Supercond. Sci. Technol. **11**, 399 (1998).

[23] M. Chandran and P. Chaddah, Supercond. Sci. Technol. **8**, 774 (1995).

[24] K. H. Müller, C. Andrikis, H. K. Liu, and S. X. Dou, Phys. Rev. B **50**, 10 218 (1994).

[25] J. Paasi, M. Lahtinen, J.-T. Eriksson, and M. Polak, Physica C **259**, 1 (1996).

[26] M. Tinkham, *Introduction to Superconductivity* 2nd ed. (McGraw-Hill, New York, 1996).

[27] E. Weber, *Electromagnetic Fields* (Wiley, New York, 1954).

[28] J. Stillwell, *Classical Topology and Combinatorial Group Theory* (Springer-Verlag, New York, 1995).

[29] L. Kettunen, K. Forsman, and A. Bossavit, IEEE Trans. Magn. **35**, 1466 (1999).

[30] R. Albanese and G. Rubinacci, IEE Proc., Part A: Phys. Sci., Meas. Instrum., Manage. Educ. **135**, 457 (1988).

[31] Generally: tree=a maximal set of cells without any cycles, cycle=set of cells without a boundary, and a path associated to a co-tree cell=the set of tree cells that together with the co-tree cell makes up a cycle.